Measuring the Deviation from the Linear and Deterministic Bias through Cosmic Gravitational Lensing Effects

Zuhui Fan[1,2,3]

ABSTRACT

Since gravitational lensing effects directly probe inhomogeneities of dark matter, lensing-galaxy cross-correlations can provide us important information on the relation between dark matter and galaxy distributions, i.e., the bias. In this paper, we propose a method to measure the stochasticity/nonlinearity of the galaxy bias through correlation studies of the cosmic shear and galaxy number fluctuations. Specifically, we employ the aperture mass statistics M_{ap} to describe the cosmic shear. We divide the foreground galaxy redshift $z_f < z_s$ into several bins, where z_s is the redshift of the source galaxies, and calculate the quantity $< M_{ap}N_g(z_f) >^2 / < N_g^2(z_f) >$ for each redshift bin. Then the ratio of the summation of $< M_{ap}N_g(z_f) >^2 / < N_g^2(z_f) >$ over the bins to $< M_{ap}^2 >$ gives a measure of the nonlinear/stochastic bias. Here $N_g(z_f)$ is the projected surface number density fluctuation of foreground galaxies at redshift z_f, and M_{ap} is the aperture mass from the cosmic-shear analysis. We estimate that for a moderately deep weak-lensing survey with $z_s = 1$, source galaxy surface number density $n_b = 30$ gal/ arcmin^2 and a survey area of 25 deg^2, the effective r-parameter that represents the deviation from the linear and deterministic bias is detectable in the angular range of $1'$-$10'$ if $|r-1| \gtrsim 10\%$. For shallow, wide surveys such as the Sloan Digital Sky Survey with $z_s = 0.5$, $n_b = 5$ gal/ arcmin^2, and a survey area of 10^4 deg^2, a 10% detection of r is possible over the angular range $1' - 100'$.

Subject headings: cosmology: theory— dark matter —galaxy: cluster: general— gravitational lensing — large-scale structure of universe

[1]Department of Astronomy, Peking University, Beijing 100871, China

[2]Beijing Astrophysical Center, Chinese Academy of Science and Peking University, Beijing 100871, China

[3]Department of Astronomy and Astrophysics, The University of Chicago, 5640 South Ellis Avenue, Chicago, IL 60637

1. Introduction

Galaxy surveys have provided us abundant knowledge of the large-scale structures of the universe. To extract cosmological information from galaxy surveys, however, it is crucial to understand the bias, i.e., the relation between the galaxy distribution and the underlying dark matter distribution (e.g., Strauss 1999 and references therein). The simplest bias model assumes a constant (in scale) bias factor between the two-point correlation of galaxies and that of dark matter: i.e.,

$$\xi_{gg}(r) = b^2\xi(r), \tag{1}$$

where ξ_{gg} is the two-point correlation function of galaxies and ξ is the two-point auto-correlation of dark matter. The b-factor is referred to as the bias factor, which can be a function of the galaxy type, brightness, etc.. The above relation is further extended to

$$\delta_g = b\delta, \tag{2}$$

where $\delta_g = \delta n/n$, the galaxy number density fluctuation, and $\delta = \delta\rho/\rho$, the dark matter mass density fluctuation. Note that relation (2) is more restrictive than relation (1) and is referred to as the linear and deterministic bias relation. Under this assumption, it is straightforward to get the dark matter clustering properties from those of galaxies since only the amplitude of clustering needs to be adjusted. In reality, the bias could be much more complex than this. The bias factor b can be scale-dependent, which would introduce complexities in converting the galaxy distribution to the underlying dark matter distribution. Further more, since galaxy formation is a complicated process, it is expected that there should be a certain level of nonlinearity and stochasticity in the relative distribution between the dark matter and galaxies (e.g., Dekel & Lahav 1999). Indeed the deviations from the linear and deterministic bias have been seen in numerical simulations (e.g., Dekel & Lahav 1999; Blanton et al. 1999). It is shown that older galaxies and the underlying dark matter are highly correlated, but younger galaxies are poorly correlated with dark matter (e.g., Blanton et al. 1999, 2000; Somerville et al. 2001)

As far as the second moments are concerned, the nonlinear/stochastic bias can be described by the quantities b and r which are defined as

$$b^2 \equiv \frac{\sigma_g^2}{\sigma^2}, \tag{3}$$

and

$$r \equiv \frac{<\delta_g\delta>}{\sigma_g\sigma}, \tag{4}$$

where $\sigma^2 \equiv <\delta^2>$ and $\sigma_g^2 \equiv <\delta_g^2>$. In the case of linear and deterministic bias, $r = 1$.

It has been proposed to measure the nonlinearity/stochasticity of the bias using the information of redshift distortions of the galaxy distribution, which are presumably caused by the underlying dark matter distribution (Dekel & Lahav 1999; Pen 1998). Tegmark and Bromley (1999) analyzed galaxy correlations in the Las Campanas Redshift Survey (Shectman et al. 1996; Bromley et al. 1998). They found that different subpopulations of galaxies are not correlated perfectly with each other, indicating that the galaxy densities and the underlying dark matter density cannot be perfectly correlated, or in other words, the bias is nonlinear/stochastic. They further showed that the deviation from the linear and deterministic bias is significant for late-type galaxies, and the r factor ranges from ~ 0.98 for very early-type galaxies to ~ 0.57 for late-type ones. However, Blanton (2000) pointed out that this large stochasticity (small r) could be the result of selection effects, and his estimation of r is $r \approx 0.95$.

Gravitational lensing effects due to large-scale structures (cosmic shear) have been becoming important probes for studying the dark matter distribution in the universe (e.g., Blandford et al. 1991; Kaiser 1992; Schneider et al. 1998; Mellier 1999; Bartelmann & Schneider 2001). Although weak ($\sqrt{<\gamma^2>}$ is on the order of $\sim 1\%$ on angular scales $< 10'$, where $<\gamma^2>$ is the top-hat variance of the cosmic shear), the cosmic-shear signals have been detected by different groups (e.g., Mellier et al. 2002 and the references there in), and useful constraints on σ_8 and Ω_0 have been set up with these lensing analyses (e.g., Maoli et al. 2001). Recently, galaxy-galaxy lensing has also been detected (Fisher et al. 2000; McKay et al. 2001; Hoekstra et al. 2002), and this enables the statistical study of properties of galactic halos and galaxy-mass correlations (e.g, Guzik & Seljak 2001, 2002).

While the most direct gain from cosmic-shear analyses is the projected dark matter distribution, or the projected power spectrum in Fourier domain (Bartelmann & Schneider 1999; van Waerbeke et al. 1999), the cross-correlation between the cosmic shear and the galaxy distribution reflects the relative distribution of dark matter and galaxies, i.e., the bias. The combination of this cross-correlation and the galaxy autocorrelation has been used to measure the scale dependency of the b-factor (van Waerbeke 1998; Hoekstra et al. 2001). Hoekstra et al. (2002) also made a first try to measure the r-factor by using the cosmic shear-galaxy, galaxy-galaxy, and cosmic shear-cosmic shear correlations. In their sample, the foreground galaxies occupy a relatively narrow redshift range. On the other hand, the mass contribution to the cosmic shear comes from a relatively broad redshift range. Therefore they need a conversion factor to convert the direct measurement result to the r-factor (see eq.[17] in Hoekstra et al. 2002). The conversion factor is model-dependent, and this adds complications to the interpretation of the observational results.

With fast developments in observations, it will be possible to divide galaxies according

to their redshifts, which can be obtained at least photometrically. This will enhance the power to extract cosmological information from lensing analyses.

In this paper, we propose to use foreground galaxies in several redshift bins with $z_f < z_s$ where z_s is the source redshift, to get a summation of $< M_{ap}N_g(z_f) >^2 / < N_g^2(z_f) >$ over the bins, which should give a good estimation of $< M_{ap}^2 >$ if the bias is linear and deterministic, i.e., $r = 1$. In other words, the ratio $[\Sigma_{z_f} < M_{ap}N_g(z_f) >^2 / < N_g^2(z_f) >]/ < M_{ap}^2 >$ measures the projected r^2-factor weighted by the power spectrum in different redshift bins. Here M_{ap} is the aperture mass used to describe cosmic shear signals, and N_g is the surface number density fluctuations of foreground galaxies. This measurement is largely independent of cosmology and of specific types of power spectra, and there is no conversion factor between r and the direct measurement result.

The rest of the paper is organized as follows. Section 2 discusses the effects of different binning of redshift of foreground galaxies on the r-estimation, i.e., the intrinsic uncertainties. In section 3 we estimate the signal-to-noise level of the measurement of r for various models. Section 4 includes discussions.

2. Redshift Binning

In this paper, the aperture-mass statistics are used in the cosmic-shear analysis (e.g., Schneider et al. 1998). The aperture mass $M_{ap}(\theta_c)$ is defined as the projected surface mass density filtered with a compensated filter function (Schneider et al. 1998)

$$M_{ap}(\theta_c) \equiv \int d^2\vec{\theta} U(\theta, \theta_c)\kappa(\vec{\theta}), \tag{5}$$

where κ is the dimensionless surface mass density, U is a compensated filter function with $U = 0$ for $\theta \geq \theta_c$. The quantity M_{ap} is related to the observable shear γ through

$$M_{ap}(\theta_c) = \int d^2\vec{\theta} Q(\theta, \theta_c)\gamma_t(\vec{\theta}), \tag{6}$$

where γ_t is the tangential component of the shear γ, and $Q(\theta, \theta_c) = (2/\theta^2)\int_0^\theta d\theta' \theta' U(\theta', \theta_c) - U(\theta, \theta_c)$.

The surface mass density κ is associated with the density perturbation along the line of sight by

$$\kappa(\vec{\theta}) = \frac{3}{2}\Big(\frac{H_0}{c}\Big)^2 \Omega_0 \int_0^{w_H} dw g(w) f_K(w) \frac{\delta(f_K(w)\vec{\theta}, w)}{a(w)}, \tag{7}$$

where H_0 is the Hubble constant, Ω_0 is the current matter density parameter of the universe, c is the speed of light, w is the comoving radial distance, w_H is the comoving radial distance to the horizon, f_K is the comoving angular diameter distance, a is the scale factor, δ is the density perturbation, and g is defined as

$$g(w) = \int_w^{w_H} dw' p_w(w') \frac{f_K(w'-w)}{f_K(w')}, \tag{8}$$

where $p_w(w)$ is the distance distribution of source galaxies, and $p_w(w)dw = p_z(z)dz$, where $p_z(z)$ is their corresponding redshift-distribution. We use the filter function of Schneider et al. (1998), which has the form $U(\theta,\theta_c) = u(\theta/\theta_c)/\theta_c^2$ with $u(x) = 0$ for $x > 1$, and $Q(\theta,\theta_c) = q(\theta/\theta_c)/\theta^2$,

$$u(x) = \frac{(l+2)^2}{\pi}(1-x^2)^l\Big(\frac{1}{l+2} - x^2\Big),$$

and

$$q(x) = \frac{(1+l)(2+l)}{\pi}x^2(1-x^2)^l,$$

with l an integer.

Then in the Fourier domain, we have

$$< M_{ap}^2(\theta_c) >= \frac{9\pi}{2}\Big(\frac{H_0}{c}\Big)^4\Omega_0^2\int_0^{w_H} dw \frac{g^2(w)}{a^2(w)} \times \int ds\ s\ P\Big(\frac{s}{f_K(w)}, w\Big)\ I_l^2(s\theta_c), \tag{9}$$

where P is the three-dimensional power spectrum of density fluctuations at the time corresponding to w, and I_l is defined as

$$I_l(\eta) = \int_0^1 dx\ x\ u(x)J_0(x\eta) = \frac{2^l\Gamma(l+3)}{\pi}\eta^{-(l+1)}J_{l+3}(\eta).$$

In the following we will use $l = 1$, and then

$$I(\eta) = \frac{2\Gamma(4)}{\pi}\eta^{-2}J_4(\eta). \tag{10}$$

In comparison with the top-hat window function, the compensated filter function (10) is very localized with a peak at $\eta \sim 4$, and therefore $< M_{ap}^2(\theta_c) >$ provides a good measurement on the power spectrum of projected density fluctuations at scale $s \sim 4/\theta_c$ (Bartelmann & Schneider 1999). When the cross-correlation between M_{ap} and the foreground-galaxy distribution is considered, the narrowness of the redshift distribution of foreground galaxies makes the cross-correlation signals come from a well-defined cosmic time. Thus, in conjunction with I^2, the contributions of the mass distribution to the cross-correlation peak at a well-defined scale $k \approx (4/\theta_c)/f_K(z_f)$, where z_f is the peak redshift of foreground galaxies and $f_K(z_f)$ is

the angular diameter distance to z_f. This property has been used in studying the scale dependence of r/b through the measurement of the lensing-foreground-galaxy cross-correlation and the auto-correlation of foreground-galaxy distributions (Schneider 1998, van Waerbeke 1998). In the analysis presented in this paper, we also use this property as explained in the following.

The projected distribution of foreground galaxies is described by

$$N_g(\vec{\theta}) = \frac{N(\vec{\theta}) - \bar{N}}{\bar{N}}, \tag{11}$$

where $N(\vec{\theta})$ is the surface number density of galaxies in the direction $\vec{\theta}$, and $\bar{N}$ is the mean surface number density of galaxies. Then the cross-correlation of M_{ap} and N_g is

$$< M_{ap}(\theta_c)N_g(\theta_c) >= 3\pi\Big(\frac{H_0}{c}\Big)^2\Omega_0\ b\ r\int dw\frac{p_f(w)g(w)}{a(w)f_K(w)}\int ds\ s\ P\Big(\frac{s}{f_K(w)}, w\Big)I^2(s\theta_c), \tag{12}$$

and the auto correlation of N_g is

$$< N_g^2(\theta_c) >= 2\pi b^2\int dw\frac{p_f^2(w)}{f_K^2(w)}\int ds\ s\ P\Big(\frac{s}{f_K(w)}, w\Big)I^2(s\theta_c), \tag{13}$$

where p_f is the foreground-galaxy distribution, b and r are the bias factors discussed in the section 1, and $r = 1$ if the bias is linear and deterministic.

As stated before, if p_f is highly peaked at z_f, then

$$< M_{ap}(\theta_c)N_g(\theta_c) > \propto 3\pi\Big(\frac{H_0}{c}\Big)^2\Omega_0\ b\ r\frac{g(z_f)}{a(z_f)f_K(z_f)}P(k, z_f), \tag{14}$$

and

$$< N_g^2(\theta_c) > \propto 2\pi b^2\frac{p_f(z_f)(dz/dw)_{z_f}}{f_K^2(z_f)}P(k, z_f), \tag{15}$$

with $k \approx (4/\theta_c)/f_K(z_f)$. Notice that in equations (14) and (15), we use z_f instead of w to label the time, and the formulation for g and f_K should be changed accordingly in the numerical calculations. Then

$$\frac{[< M_{ap}(\theta_c)N_g(\theta_c) >]^2}{< N_g^2(\theta_c) >} \times p_f(z_f)\ \propto r^2\Big\{\frac{9\pi}{2}\Big(\frac{H_0}{c}\Big)^4\Omega_0^2\frac{g^2(z_f)}{a^2(z_f)}\Big(\frac{dw}{dz}\Big)_{z_f}P(k, z_f)\Big\}. \tag{16}$$

From equation (9), it is seen that

$$< M_{ap}^2(\theta_c) > \propto \Big[\frac{9\pi}{2}\Big(\frac{H_0}{c}\Big)^4\Omega_0^2\int dz\frac{g^2(z)}{a^2(z)}\Big(\frac{dw}{dz}\Big)_z P(k, z)\Big],$$

with $k \approx (4/\theta_c)/f_K(z)$. Therefore if the foreground galaxies are divided into several redshift bins with $z_f \leq z_s$, and $[< M_{ap}(\theta_c)N_g(\theta_c) >]^2/ < N_g^2(\theta_c) >$ is calculated for each bin, the summation of $[< M_{ap}(\theta_c)N_g(\theta_c) >]^2/ < N_g^2(\theta_c) > \times p_f(z_f)$ over the bins would give rise to an estimation of $< M_{ap}^2(\theta_c) >$ if $r = 1$. With $r \neq 1$, then we have

$$\Sigma_{z_f}\Big\{\frac{[< M_{ap}(\theta_c)N_g(\theta_c, z_f) >]^2}{< N_g^2(\theta_c, z_f) >}p_f(z_f)\Delta z_f\Big\} \approx r^2 < M_{ap}^2(\theta_c) >,$$

or

$$r^2 \approx \frac{\Sigma_{z_f}\Big\{[< M_{ap}(\theta_c)N_g(\theta_c, z_f) >]^2/ < N_g^2(\theta_c, z_f) > \times p_f(z_f)\Delta z_f\Big\}}{< M_{ap}^2(\theta_c) >}. \qquad (17)$$

Here we have explicitly written down the redshift dependence of N_g. The approximate sign " $\approx$ " means that when equation (17) is used in estimating r, there are intrinsic uncertainties depending on the redshift binning. The binning effects are discussed below. In equation (17), it is assumed that r is independent of scales. In general, r is scale-dependent, and then equation (17) provides a measurement of the power-spectrum-weighted r-factor. In addition, theoretical studies and numerical simulations showed that the r factor evolves with time, i.e., it should be a function of redshift z (e.g., Tegmark & Peebles 1998; Blanton et al. 2000; Somerville et al. 2001). Then, the method proposed here really measures the weighted averaged r over the redshift range up to z_s, the source redshift.

With $r = 1$, we expect the right hand side of equation (17) (denoted as r_{es}^2) to be close to 1 if the binning is fine enough. On the other hand, it is observationally impractical if a very fine binning is required. In the following, we study how r_{es}^2 deviates from 1 with different binning in the case of linear and deterministic bias, i.e., $r = 1$. This gives us an evaluation on the intrinsic uncertainty when we use equation (17) to measure the r-factor.

We assume all source galaxies are located at redshift z_s. The foreground-galaxy distribution is written as

$$\begin{aligned} p_f(z_f) &= \frac{1}{z_2 - z_1} \quad \text{for} \quad z_1 \leq z_f \leq z_2 \\ &= 0 \qquad\qquad \text{otherwise} \end{aligned} \qquad (18)$$

Equal binning is applied in the calculations, i.e., $(z_2 - z_1) = z_s/N_{bin}$ where N_{bin} is the number of bins used. A nonlinear power spectrum in the form of Peacock and Dodds (1996) is adopted.

Figure 1 presents the integrand of $< M_{ap}^2(\theta_c) >$ [denoted as $m_{ap}(z)$, see eq. (9) but with the integrated variable changed from w to z] with $z_s = 1$ versus redshift z. Figure 1a is for a Λ-dominated cold dark matter (ΛCDM) model with $\Omega_0 = 0.3, \Omega_\Lambda = 0.7, H_0 = 67$ km/s/Mpc,

the shape parameter $\Gamma = 0.2$, and $\sigma_8 = 0.93$. Different curves correspond to $\theta_c = 1', 3', 5'$, and $10'$, respectively. Figure 1b is for the open CDM model (OCDM) with $\Omega_0 = 0.3$, $\Omega_\Lambda = 0$, $H_0 = 67$ km/s/Mpc, $\Gamma = 0.2$, and $\sigma_8 = 0.87$. For comparison, we plot in Figure 1c the results for both models with $\theta_c = 5'$. It can be seen that the contributions to $< M_{ap}^2(\theta_c) >$ spread over a fairly large range of z. For OCDM, the low redshift contributions are more prominent than those of the ΛCDM model.

In Figure 2 we show $1 - r_{es}^2$ (assuming linear and deterministic bias) with $z_s = 1$ versus θ_c for the ΛCDM model with $N_{bin} = 5, 10,$ and 20, which corresponds to $\Delta z = z_2 - z_1 = 0.2,\ 0.1,$ and 0.05, respectively. We see that with $\Delta z = 0.2$, the deviation of r_{es}^2 from 1 is as high as about 10%, and $1 - r_{es}^2$ reaches $\sim 7\%$ at $20'$. Thus with $N_{bin} = 5$, the accuracy is not good enough to give a sound estimation of r by using equation (17). With $N_{bin} = 10$ and $\Delta z = 0.1$, $1 - r_{es}^2 < 3\%$ for the whole angular range we studied, and at $\sim 20'$, r_{es}^2 deviates from 1 by only less than 2%. With finer binning of $\Delta z = 0.05$, $1 - r_{es}^2 < 0.7\%$ for angular scales up to $100'$ with $1 - r_{es}^2 < 0.5\%$ around $20'$. Therefore, with $\Delta z = 0.05$, the intrinsic uncertainty of equation (17) is tiny, but observationally, it may be difficult to precisely (with 0.05 accuracy) measure the redshift for a large number of foreground galaxies especially for those with redshift close to 1, since most likely only photometric redshifts will be available for high-redshift galaxies. Considering both the intrinsic uncertainties and the observational realities, it is therefore optimal to use $N_{bin} = 10$ ($\Delta z = 0.1$) in the case of $z_s = 1$.

Similar curves for the OCDM model are shown in Figure 3. It is seen that $1 - r_{es}^2$ is larger for the OCDM model than the corresponding $1 - r_{es}^2$ for the ΛCDM model. This is because as seen in Figure 1c, low-redshift contributions to $< M_{ap}^2 >$ are more significant in the OCDM model than in the ΛCDM model, and therefore for OCDM, relatively finer binning is needed in low redshifts in order to reach the same $1 - r_{es}^2$ as that of ΛCDM. Still, however, with $N_{bin} = 10$ ($\Delta z = 0.1$), $1 - r_{es}^2$ is small enough with $1 - r_{es}^2 < 3.5\%$ at $20'$, and $1 - r_{es}^2 \leq 4\%$ for the whole angular range up to $100'$.

In Figure 4 we plot $1 - r_{es}^2$ for the ΛCDM model (*Solid lines*) and OCDM model (*dashed lines*) with $z_s = 1.5$. The two sets of curves correspond, respectively, to $N_{bin} = 10$ ($\Delta z = 0.15$) and $N_{bin} = 15$ ($\Delta z = 0.1$). For $N_{bin} = 10$ ($\Delta z = 0.15$), $1 - r_{es}^2 < 3.5\%$ and 5% for the ΛCDM model and OCDM model, respectively. At 20 arcmin, $1 - r_{es}^2 < 2.5\%$ and 4% for the respective two models. For $N_{bin} = 15$ ($\Delta z = 0.1$), the deviations of r_{es}^2 from 1 are, respectively, less than 1.5% and 2% for the two models for the whole angular range considered. Thus for $z_s = 1.5$, $N_{bin} = 15$ ($\Delta z = 0.1$) guarantees that the intrinsic uncertainties in terms of r estimation with equation (17) are small. Even with $N_{bin} = 10$ ($\Delta z = 0.15$), the intrinsic uncertainties are insignificant.

Figure 5 shows the curves for $z_s = 0.5$. The results for each of the two models with

$N_{bin} = 5$ ($\Delta z = 0.1$) and $N_{bin} = 10$ ($\Delta z = 0.05$) are shown in the plot. For $N_{bin} = 5$ and $\Delta z = 0.1$, the deviations are relatively large, with $1-r_{es}^2$ as high as 8% and 10% for the ΛCDM model and OCDM model, respectively. With $N_{bin} = 10$ and $\Delta z = 0.05$, the deviations are less than 2% and 3% for ΛCDM and OCDM, respectively, with $1-r_{es}^2 < 1.5\%$ and 2% at $20'$. Therefore, for $z_s = 0.5$, it is necessary to go to $\Delta z = 0.05$ in order to control the intrinsic uncertainties in the r-estimation using equation (17). Fortunately, for $z \leq 0.5$, the redshifts of foreground galaxies can be obtained spectroscopically with very high precision, and it is possible to bin them down to $\Delta z = 0.05$.

From above analyses, we see that for source galaxies at z_s, in general 10 bins for the foreground galaxies would be enough to control the intrinsic uncertainties of equation (17) to a reasonably low level. For $z_s \geq 1$, the intrinsic uncertainties can be well controlled if the bin interval $\Delta z = 0.1$ is used.

3. Signal-to-Noise Ratio

In this section, we discuss the signal-to-noise ratio of r estimated with equation (17) considering the intrinsic ellipticity of source galaxies, Poisson noise of the foreground-galaxy distribution, and the cosmic variance.

If we denote

$$\{[< M_{ap}(\theta_c)N_g(\theta_c, z_f) >]^2 / < N_g^2(\theta_c, z_f) >\} p_f(z_f)\Delta z_f$$

as $M_{z_f}^2$, then equation (17) becomes

$$r^2 \approx \frac{\Sigma_{z_f} M_{z_f}^2}{< M_{ap}^2(\theta_c) >}. \tag{19}$$

To estimate the signal-to-noise ratio of r, we assume that the M_{z_f} of different redshift bins are independent. This is a reasonable assumption with the bin intervals we considered. Further we assume that the dispersion of $< N_g^2(\theta_c, z_f) >$ can be neglected (van Waerbeke 1998). For one field, we then have

$$\frac{\sigma(M_{z_f}^2)}{M_{z_f}^2} = \frac{2\sigma(< M_{ap}(\theta_c)N_g(\theta_c, z_f) >)}{< M_{ap}(\theta_c)N_g(\theta_c, z_f) >}, \tag{20}$$

and

$$\sigma^2(\Sigma_{z_f} M_{z_f}^2) = \Sigma_{z_f}\sigma^2(M_{z_f}^2). \tag{21}$$

If $\Sigma_{z_f}(M_{z_f}^2)$ and $< M_{ap}^2(\theta_c) >$ are independent, then

$$\frac{\sigma(r^2)}{r^2} = \Big\{ \frac{\sigma^2(\Sigma_{z_f} M_{z_f}^2)}{(\Sigma_{z_f} M_{z_f}^2)^2} + \frac{\sigma^2(< M_{ap}^2(\theta_c) >)}{[< M_{ap}^2(\theta_c) >]^2} \Big\}^{1/2}. \tag{22}$$

However, it is likely that $\Sigma_{z_f}(M_{z_f}^2)$ and $< M_{ap}^2(\theta_c) >$ are not independent, so then (Taylor 1982)

$$\frac{\sigma(r^2)}{r^2} \leq \sigma_{max} = \frac{\sigma(\Sigma_{z_f} M_{z_f}^2)}{\Sigma_{z_f} M_{z_f}^2} + \frac{\sigma(< M_{ap}^2(\theta_c) >)}{< M_{ap}^2(\theta_c) >}. \tag{23}$$

In the following, both equation (22) and σ_{max} defined in equation (23) are calculated.

We use the estimation of van Waerbeke (1998) to calculate $\sigma[< M_{ap}(\theta_c) N_g(\theta_c, z_f) >]$, i.e.,

$$\sigma(< M_{ap}(\theta_c) N_g(\theta_c, z_f) >) = \Big[< M_{ap}^2(\theta_c) > + \frac{G\sigma_\epsilon^2}{2N_b} \Big]^{1/2} \Big[< N_g^2(\theta_c, z_f) > + \frac{\tilde{G}}{N_f} \Big]^{1/2}, \tag{24}$$

where N_b and N_f are the numbers of source and foreground galaxies in one field, respectively, σ_ϵ represents the intrinsic ellipticity of source galaxies, $G = \pi\theta_c^2 \int d^2\theta Q^2(\theta, \theta_c) = 6/5$ if the compensated filter defined previously with $l = 1$ is used, and $\tilde{G} = \pi\theta_c^2 \int d^2\theta U^2(\theta, \theta_c) = G$. Within each pair of square brackets of the right-hand side of equation (24), the first term represents the uncertainty due to the cosmic variance. For the aperture mass, the intrinsic ellipticity of background galaxies contributes to the uncertainty through the second term of the first square bracket. The second term in the second square bracket represents the statistical uncertainty due to the finite number of foreground galaxies.

For $\sigma(< M_{ap}^2 >)$, we have (Schneider et al. 1998)

$$\sigma(< M_{ap}^2 >) \approx \Big[\mu_4 < M_{ap}^2 > + \Big(\frac{\sigma_\epsilon^2 G}{\sqrt{2} N_b} + \sqrt{2} < M_{ap}^2 > \Big) \Big]^{1/2}, \tag{25}$$

where μ_4 is the kurtosis of M_{ap} with $\mu_4 =< M_{ap}^4 > /(< M_{ap}^2 >)^2 - 3$, which is 0 if M_{ap} is Gaussian. On small scales, however, non-linear effects are strong, and M_{ap} is non-Gaussian. As shown in van Waerbeke (2002), $< M_{ap}^4 > / < M_{ap}^4 >_{Gaussian}$ can reach about 7 for $\theta_c \leq 3'$ for ΛCDM model. On the other hand, on small scales, we expect statistical uncertainties to dominate over the cosmic variance, thus, neglecting non-Gaussianity should not affect the error estimation significantly. In the following, we ignore the μ_4 term in equation (25).

Figure 6 shows $\sigma(r^2)/r^2$ of one field with $z_s = 1$, $N_{bin} = 10$ ($\Delta z = 0.1$), $n_b = 30$ gal/ arcmin^2, $\sigma_\epsilon = 0.2$ and $n_f = 5$ gal/ arcmin^2, where n_b and n_f are the surface number

densities of background and foreground galaxies, respectively. The solid lines are for the ΛCDM model, and the dashed lines are for the OCDM model. In each model, the upper line corresponds to the result of σ_{max} in equation (23) and the lower line corresponds to that of equation (22). It is seen that at $\theta_c \leq 3'$, the statistical uncertainties are dominant, and $\sigma(r^2)/r^2$ is larger for the ΛCDM model. At angular scales $\theta_c > 3'$, the two models have about the same $\sigma(r^2)/r^2$, and it approaches a constant when $\theta_c > 10'$.

In Figure 7 we plot $\sigma(r^2)/r^2$ for a survey of 25 deg^2. The meanings of different lines are the same as those in Figure 6. We see that $\sigma(r^2)/r^2 \leq 20\%$ or $\sigma(r)/r = 1/2\sigma(r^2)/r^2 \leq 10\%$ for $\theta_c \leq 10'$. In other words, the deviation of r from 1 is detectable if it is larger than 10% at $\theta_c \leq 10'$. Going deep in a survey, the number density of source galaxies increases and the statistical uncertainties decrease. As we have seen, however, on relatively large scales, the cosmic variance dominates, and thus a deeper survey will not help to increase the precision on the determination of r on those scales. On the other hand, by increasing the survey area, $\sigma(r^2)/r^2$ decreases by a same factor over the whole angular range. In Figure 8, we compare the effects on $\sigma(r^2)/r^2$ with a deeper survey and with a wider survey for the ΛCDM model. The solid line shows the result of equation (22) with $n_b = 30$ gal/ arcmin^2 and a survey area of 25 deg^2. The dashed line is for $n_b = 60$ gal/ arcmin^2 and a survey area of 25 deg^2. The dot-dashed line is for $n_b = 30$ gal/ arcmin^2 and a survey area of 100 deg^2. It is clearly seen that in terms of determining r, it is more effective to go wide than to go deep in a lensing survey.

Figure 9 shows the results for $z_s = 1.5$ and $N_{bin} = 15$ ($\Delta z = 0.1$). The other parameters are the same as in Figure 7. At small angular scales, ($\theta_c \leq 4'$), $\sigma(r^2)/r^2$ is smaller in the case of $z_s = 1.5$ because of relatively large cosmic-shear signals compared $z_s = 1$. A 10% detection is reachable for $\theta_c \leq 10'$ with a survey of 25 deg^2.

In the case of $z_s = 0.5$, since the shear signals are very weak, the statistical uncertainties are relatively very large. Figure 10 plots $\sigma(r^2)/r^2$ for $n_b = 30$ gal/ arcmin^2, $N_{bin} = 10$ ($\Delta z = 0.05$) and a survey area of 25 deg^2 for the two cosmological models. The number density of foreground galaxies is $n_f = 5$ gal/ arcmin^2. We see that over the whole angular range, $\sigma(r^2)/r^2 > 20\%$. The good strategy is then to do shallow, wide surveys. For the Sloan Digital Sky Survey (SDSS), the survey area can be as large as 10^4 deg^2. The surface number density of source galaxies is about a few (e.g., Mckay et al. 2001). In Figure 11 we show $\sigma(r^2)/r^2$ for $n_b = 5$ gal/ arcmin^2 and a survey area of 10^4 deg^2. All the other parameters are the same as in Figure 10. It is seen that with such a large survey area, a 10% detection of r is possible for all the angular scales we considered ($1' - 100'$).

We would like to emphasize that in this section we only aimed at giving an estimation on the signal-to-noise ratio of r, i.e., to what level the deviation of r from 1 is detectable. For

that, we only calculated the standard deviation of r. Since the statistics of r are certainly non-Gaussian, and rather complicated, strictly speaking we cannot draw conclusions on the significance level of a measured r based on Gaussian statistics. For example, if we get a 2σ measurement on r, the Gaussian probability that r is consistent with $r = 1$ is 5%. For real r, the probability can be very different depending on the statistics of r. Nonetheless, we expect that our signal-to-noise ratio should give a reasonable estimation of the detectability of r. Detailed statistical properties of r can be best studied through numerical simulations, which is our planned next step. In addition, in our estimation, we implicitly assumed that the uncertainties were small, so that the error propagation rules were applicable. From our calculations discussed above, the uncertainties are indeed small on the angular range of less than $< 10'$ if the survey area is large enough.

4. Discussion

In this paper, we studied the feasibility of extracting information on r from the cross-correlation between the foreground-galaxy distribution and cosmic gravitational lensing effects under the availability of the redshift information for each foreground galaxy. We showed that for $z_s \sim 1$, the intrinsic uncertainty in the r-estimation can be well controlled if the foreground galaxies are binned with $\Delta z = 0.1$. This binning requirement is within the accuracy range of photometrically determined redshifts, and is thus achievable. For shallow surveys with $z_s \sim 0.5$, a fine binning with $\Delta z = 0.05$ is necessary. This fine binning is possible, since the redshifts of low-redshift galaxies can be obtained spectroscopically.

We further found that for a moderately deep lensing survey with $z_s \sim 1$ and $n_b = 30$ gal/ arcmin^2, a 10% detection on $|r - 1|$ is possible in the angular range of $1' - 10'$ with a survey area of 25 deg^2. A deeper survey with $n_b = 60$ gal/ arcmin^2 helps to reduce uncertainties only on small angular scales where the noise due to the intrinsic ellipticity of source galaxies dominates. The effective way to reduce the uncertainties over a large angular range is to increase the survey area. For example, with a survey area of 100 deg^2, a 10% detection of $|r - 1|$ can be made up to $\theta_c \approx 20'$.

For $z_s = 0.5$, because of the relatively low cosmic shear signal, the statistical noise from the intrinsic ellipticity of source galaxies is much more dominant than in the case of $z_s \sim 1$. Thus a very large survey area is needed in order to detect the deviation of r from 1. SDSS will eventually have a survey area of about 10^4 deg^2, and will be very suitable to be used to measure r with the method we propose here.

For the ΛCDM model, the lensing effects on source galaxies with $z_s = 1$ mainly come

from the matter distribution around redshift $z \sim 0.18 - 0.68$, with a peak located at $z \sim 0.4$ for $\theta_c = 1'$. The three-dimensional wave-vector k corresponding to $z \sim 0.4$ and $\theta_c = 1'$ is $k \sim 12(\ \mathrm{Mpc}h^{-1})^{-1}$. For $\theta_c = 10'$, the contributions to the lensing effects peak at $z \sim 0.29$, with significant amounts from $z \sim 0.1 - 0.57$. The corresponding peak scale is $k \sim 1.7(\ \mathrm{Mpc}h^{-1})^{-1}$. Thus, measuring r in the angular scale range $1' - 10'$ with $z_s = 1$, we probe the bias of structure distribution on scales of about 0.05 $\mathrm{Mpc}h^{-1}$ to about 1 $\mathrm{Mpc}h^{-1}$ at redshift $z \sim 0.1 - 0.7$. For $z_s = 0.5$, the lensing effects are mainly from matter fluctuations in the redshift range $z \sim 0.08 - 0.4$ for $\theta_c = 1' - 10'$. The corresponding scale is ~ 0.06 $\mathrm{Mpc}h^{-1}$ to ~ 0.6 $\mathrm{Mpc}h^{-1}$.

In the above studies, we have assumed that source galaxies are all located at the same redshift z_s. For future surveys, it is possible to bin source galaxies according to their redshifts, and thus our analyses here will be directly applicable. Currently, most surveys select source galaxies according to their luminosities. Their redshift distribution is approximately in the form $p_b(z) \propto z^2 exp[-(z/z_0)^\beta]$ with $\beta \approx 1.5$. In this case, in order to control well the intrinsic uncertainties in the r-estimation, the redshift range of foreground galaxies has to be extended to about $< z >= 1.5 z_0$. With $z_0 = 0.7$, $< z > \approx 1$.

With the fast growth of gravitational lensing surveys, we expect, with the additional information on the galaxy distribution, that we can obtain a great deal of knowledge on the process of galaxy formation, which will further help us to extract cosmological information from other types of surveys.

We thank the referee for the constructive comments that helped us further clarify our studies. This research was supported by the National Science Foundation of China, under Grant 10243006.

REFERENCES

Bartelmann, M., & Schneider, P. 1999, A&A, 345, 17

Bartelmann, M., & Schneider, P. 2001, Phys. Rep., 340, 291

Blandford, R. D., Saust, A. B., Brainerd, T. G., & Villumsen, J. V. 1991, MNRAS, 251, 600

Blanton, M., Cen, R., Ostriker, J. P., & Strauss, M. A. 1999, ApJ, 522, 590

Blanton, M., Cen, R., Ostriker, J. P., Strauss, M. A., & Tegmark, M. 2000, ApJ, 531, 1

Blanton, M. 2000, ApJ, 544, 63

Bromley, B. C., Press, W. H., Lin, H., & Kirshner, R. P. 1998, ApJ, 505, 25

Dekel, A., & Lahav, O. 1999, ApJ, 520, 24

Fischer. P. et al. 2000, AJ, 120, 1198

Guzik, J. & Seljak, U. 2001, MNRAS, 321, 439

Guzik, J. & Seljak, U. 2002, MNRAS, 335, 311

Hoekstra, H., Yee, H. K. C. & Gladders, M. D. 2001, ApJ, 558, L11

Hoekstra, H., van Waerbeke, L., Gladders, M. D., Mellier, Y., & Yee, H. K. C. 2002, ApJ, 577, 604

Hoekstra, H.. Franx, M., Kuijken, K., Carlberg, R. G., & Yee, H. K. C. 2002, astro-ph/0211633

Kaiser, N. 1992, ApJ, 388, 272

Maoli, R. et al. 2001, A&A, 368, 766

McKay, T. et al. 2001, astro-ph/0108013

Mellier, Y. 1999, ARA&A, 37, 127

Mellier, Y., van Waerbeke, L., Bertin, E. & Bernardeau, F. 2002, Proc. SPIE, 4847, 112

Peacock, J. A., & Dodds, S. J. 1996, MNRAS, 280, L19

Pen, U. L. 1998, ApJ, 504, 601

Schneider, P. 1998, ApJ, 498, 43

Schneider, P., van Waerbeke, L., Jain, B., & Kruse, G. 1998, MNRAS, 296, 873

Shectman, S. A., Landy, S. D., Oemler, A., Tucker, D. L., Lin, H., Kirshner, R. P., & Schechter, P. L. 1996, ApJ, 470, 172

Somerville R. S., Lemson, G., Sigad, Y., Dekel, A., Kauffmann, G., & White, S. D. M. 2001, MNRAS, 320, 289

Strauss, M.A. 1999, in Formation of Structure in the Universe, ed. A. Dekel & J. P. Ostriker (Cambridge: Cambridge University Press), 172

Taylor, J. R. 1982, An Introduction to Error Analysis: The Study of Uncertainties in Physical Measurements (Mill Valley: University Science Books)

Tegmark, M., & Bromley, B. C. 1999, ApJ, 518, L69

Tegmark, M., & Peebles, P. J. E. 1998, ApJ, 500, L79

van Waerbeke, L. 1998, A&A, 334, 1

van Waerbeke, L., Bernardeau, F., & Mellier, Y. 1999, A&A, 342, 15

van Waerbeke, Mellier, Y., Pello, R., Pen, U-L., McCracken, H. J., & Jain, B. 2002, A&A, 393, 369

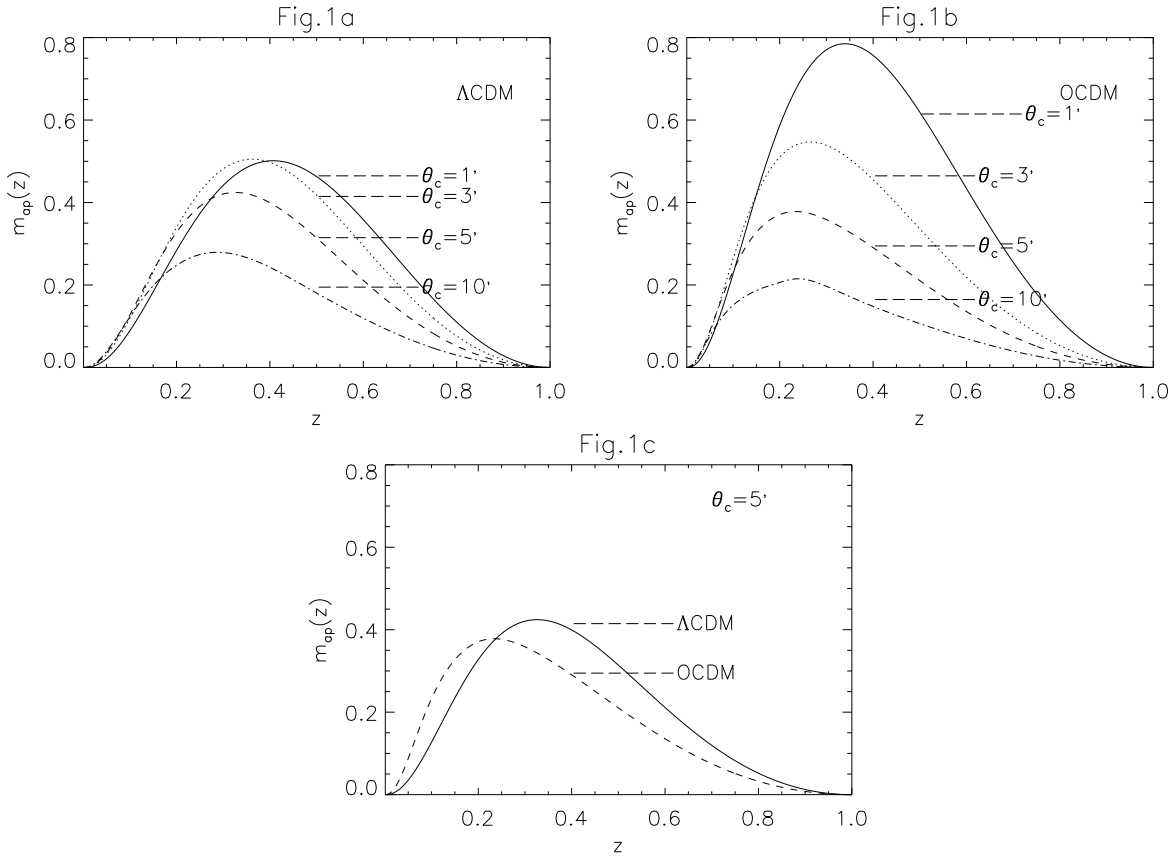

Fig. 1.— Plot of $m_{ap}(z)$, the integrand of $< M_{ap}^2 >$, vs. redshift z. (a) For the ΛCDM model. The solid line is for $\theta_c = 1'$, the dotted line is for $\theta_c = 3'$, the dashed line is for $\theta_c = 5'$, and the dot-dashed line is for $\theta_c = 10'$. (b) For the OCDM model. (c) For $\theta_c = 5'$, where the solid line is for the ΛCDM model, and the dashed line is for the OCDM model.

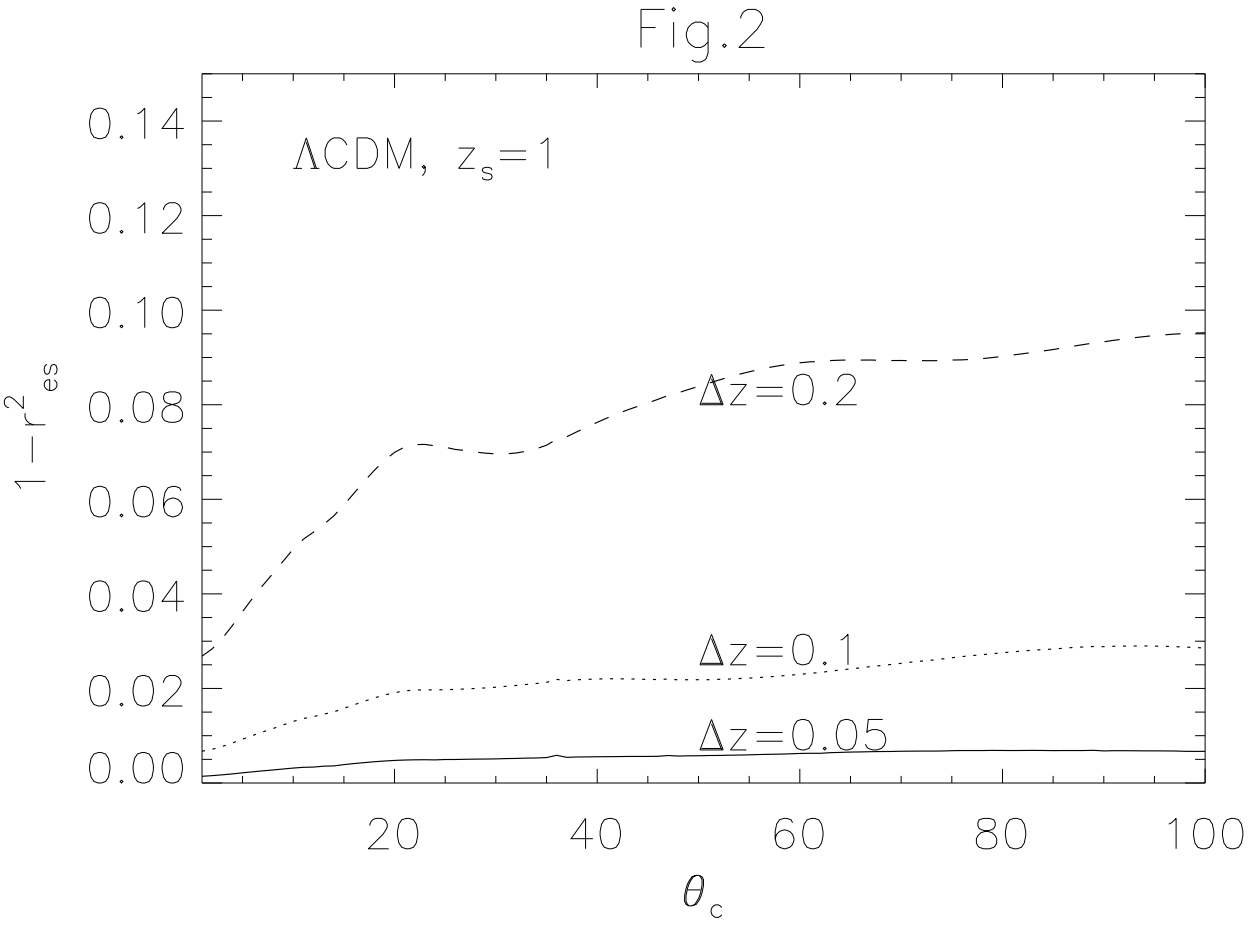

Fig. 2.— Intrinsic uncertainty $1 - r_{es}^2$ vs. the angular scale θ_c (arcmin) with $z_s = 1$ for the ΛCDM model. The solid line is for $\Delta z = 0.05$, the dotted line is for $\Delta z = 0.1$, and the dashed line is for $\Delta z = 0.2$.

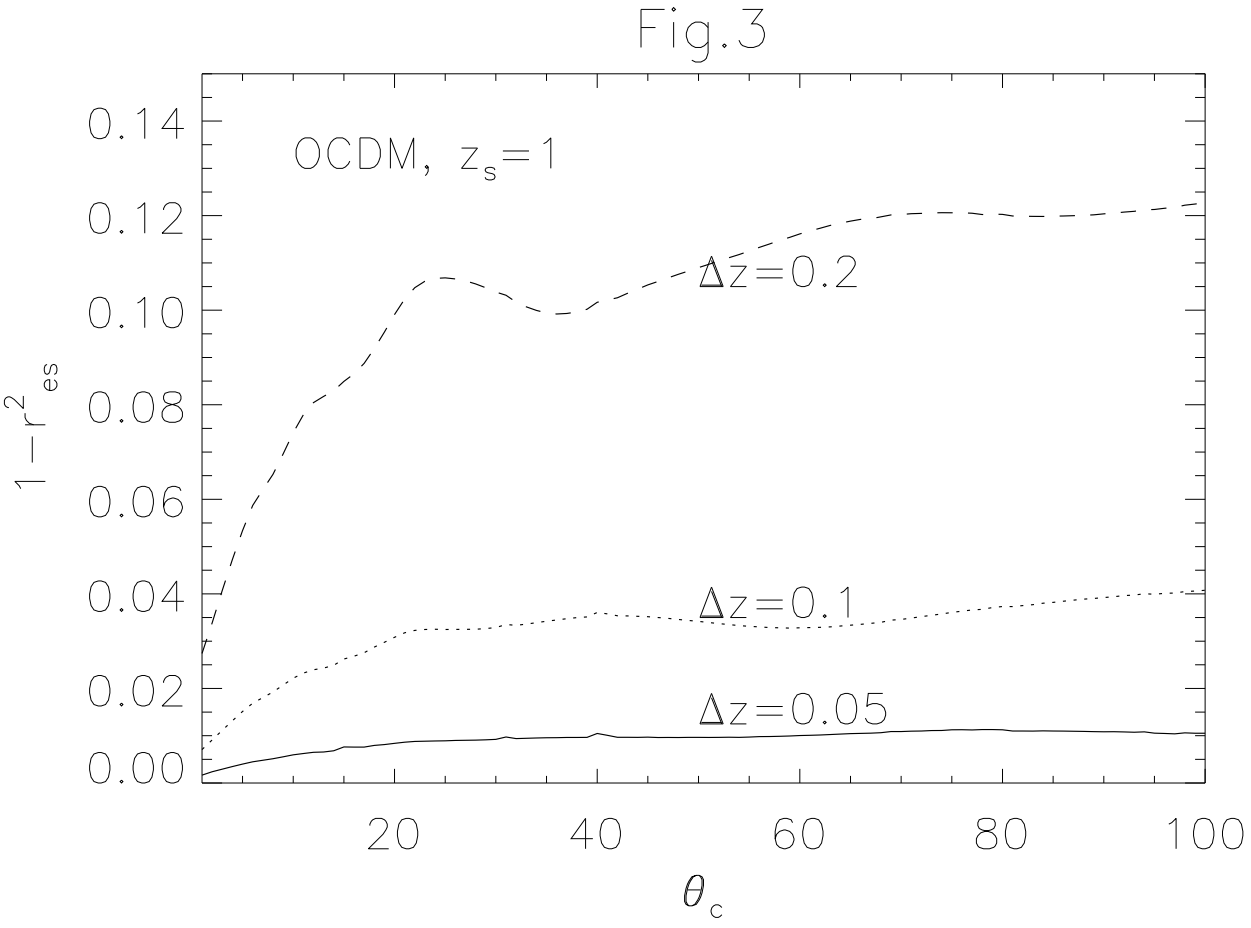

Fig. 3.— Intrinsic uncertainty $1 - r_{es}^2$ vs. the angular scale θ_c (arcmin) with $z_s = 1$ for the OCDM model. The solid line is for $\Delta z = 0.05$, the dotted line is for $\Delta z = 0.1$, and the dashed line is for $\Delta z = 0.2$.

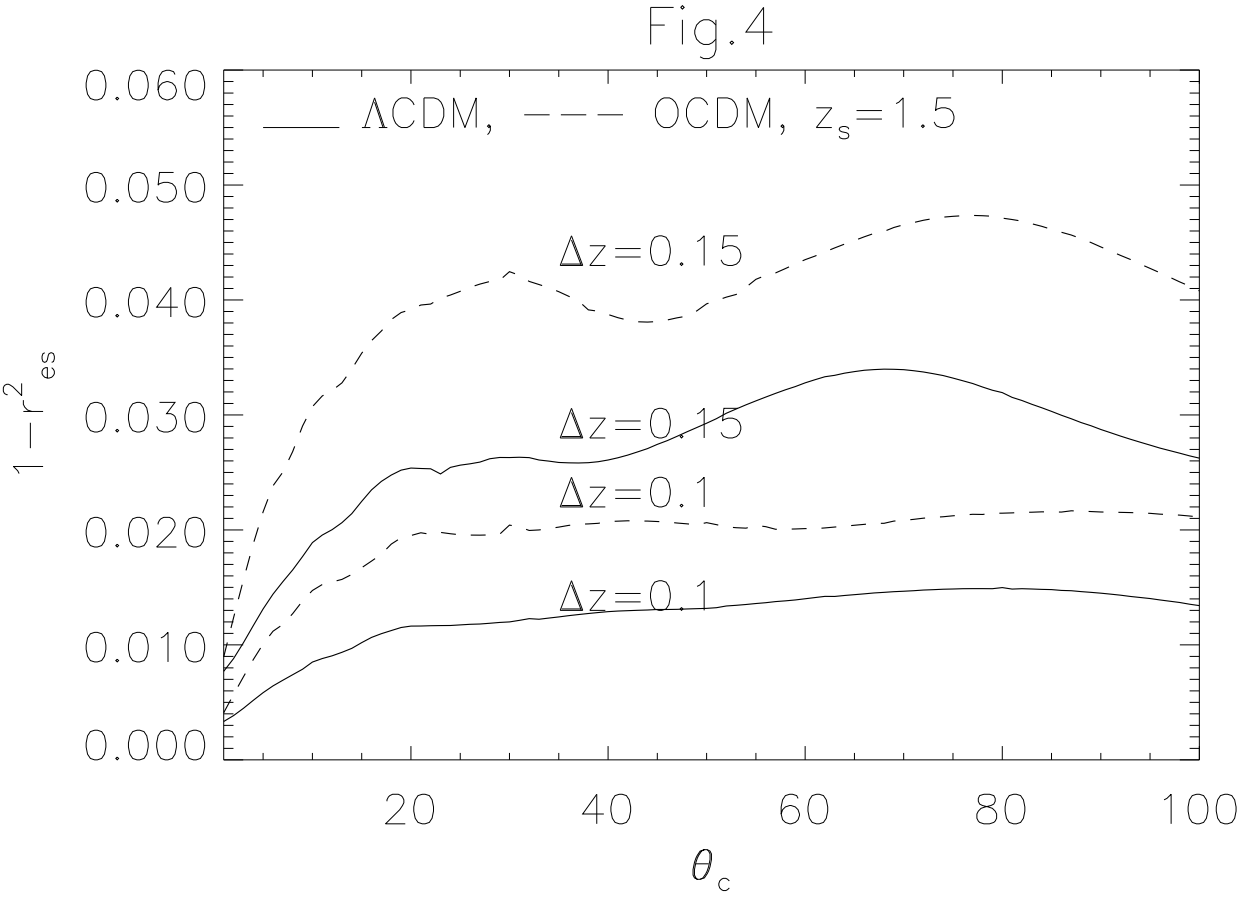

Fig. 4.— Intrinsic uncertainty $1 - r_{es}^2$ vs. the angular scale θ_c (arcmin) with $z_s = 1.5$. The solid lines are for the ΛCDM model, and the dashed lines are for the OCDM model. In each pair of lines, the upper one is for $\Delta z = 0.15$, and the lower one is for $\Delta z = 0.1$.

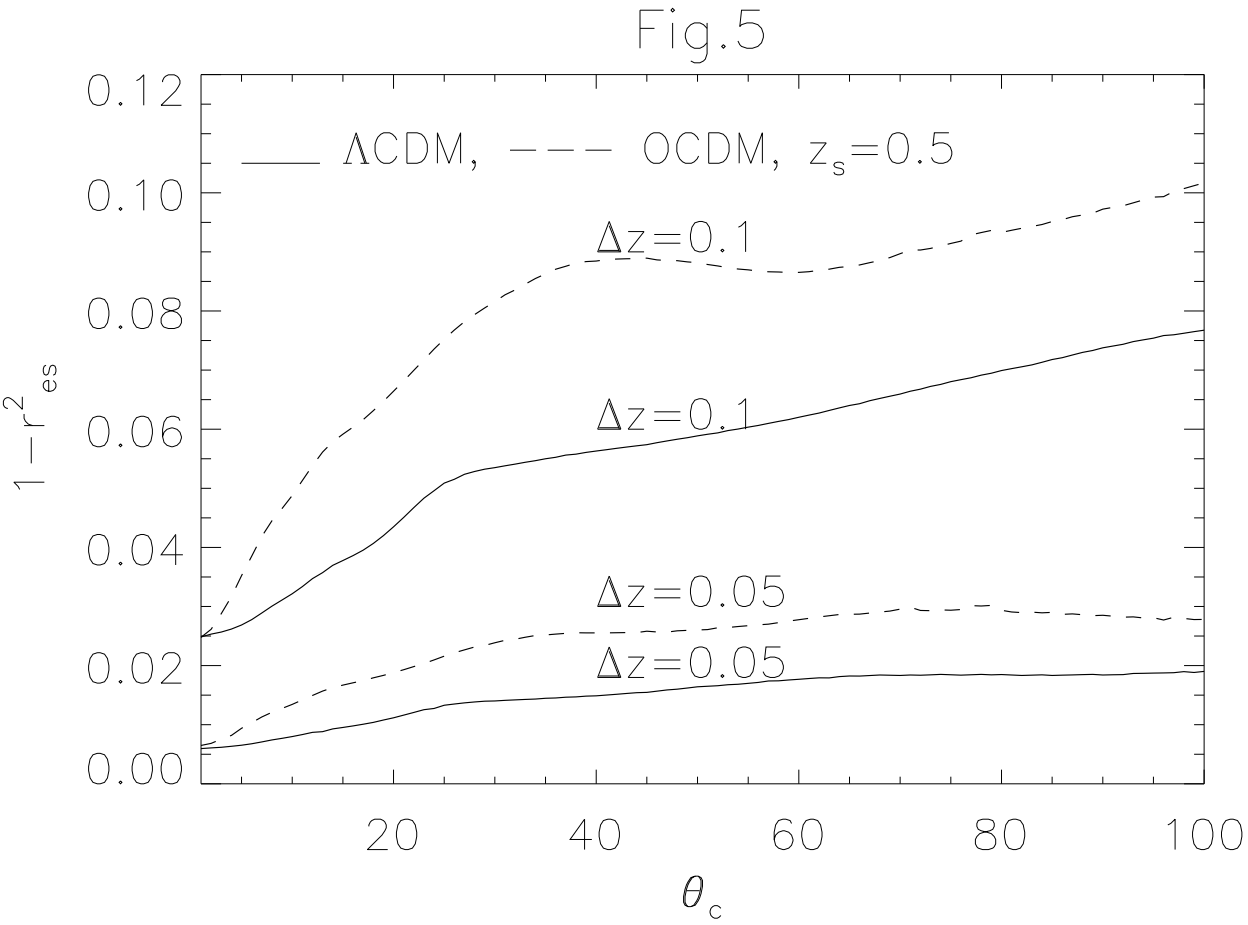

Fig. 5.— Intrinsic uncertainty $1 - r_{es}^2$ vs. the angular scale θ_c (arcmin) with $z_s = 0.5$. The solid lines are for the ΛCDM model, and the dashed lines are for the OCDM model. In each pair of lines, the upper one is for $\Delta z = 0.1$, and the lower one is for $\Delta z = 0.05$.

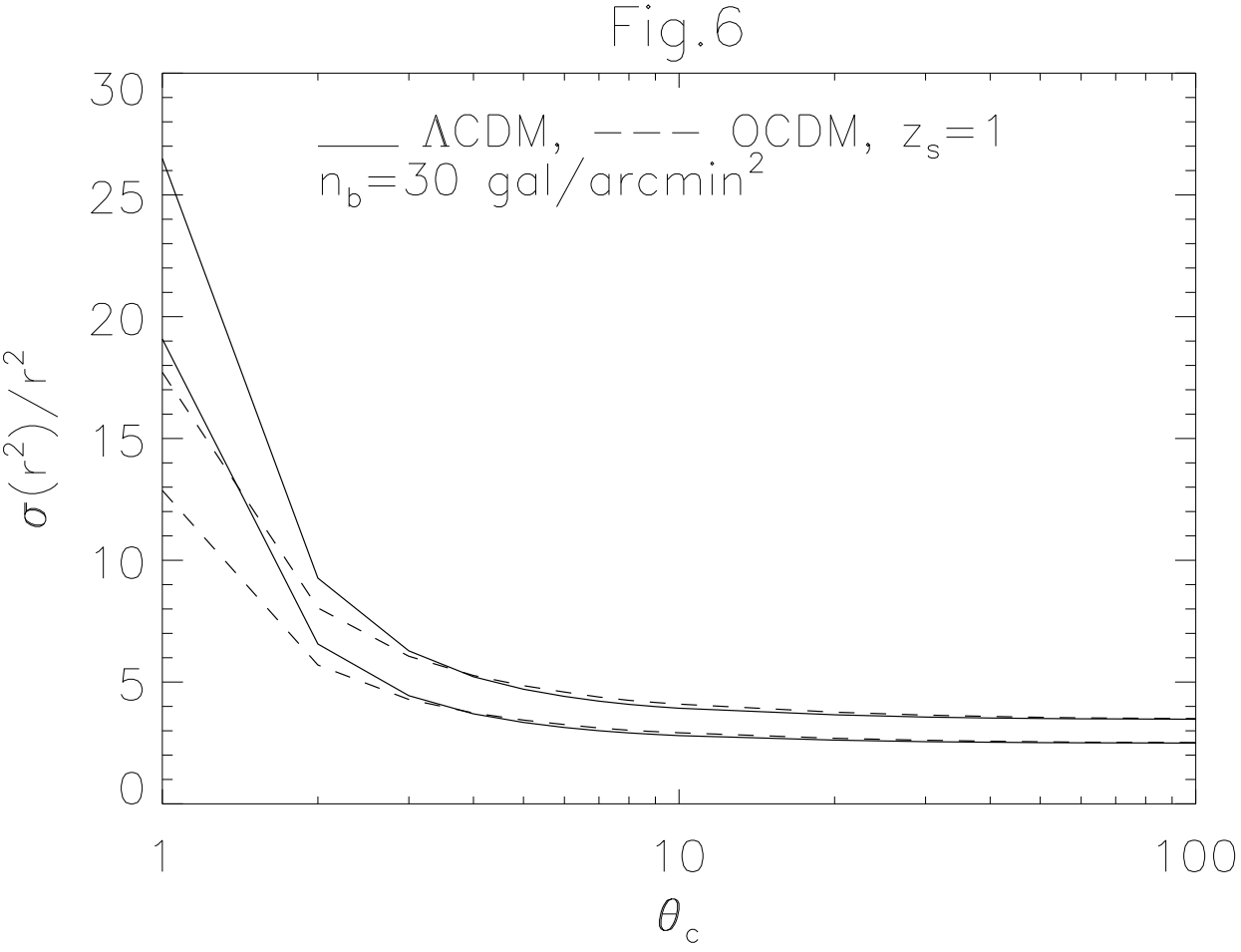

Fig. 6.— Plot of $\sigma(r^2)/r^2$ vs. θ_c (arcmin) for one field with $z_s = 1$, $n_b = 30$ gal/arcmin^2, $n_f = 5$ gal/arcmin^2, and $\sigma_\epsilon = 0.2$. The solid lines are for the ΛCDM model, and the dashed lines are for the OCDM model. In each pair of lines, the upper one corresponds to σ_{max} in eq. (23), and the lower one corresponds to eq. (22).

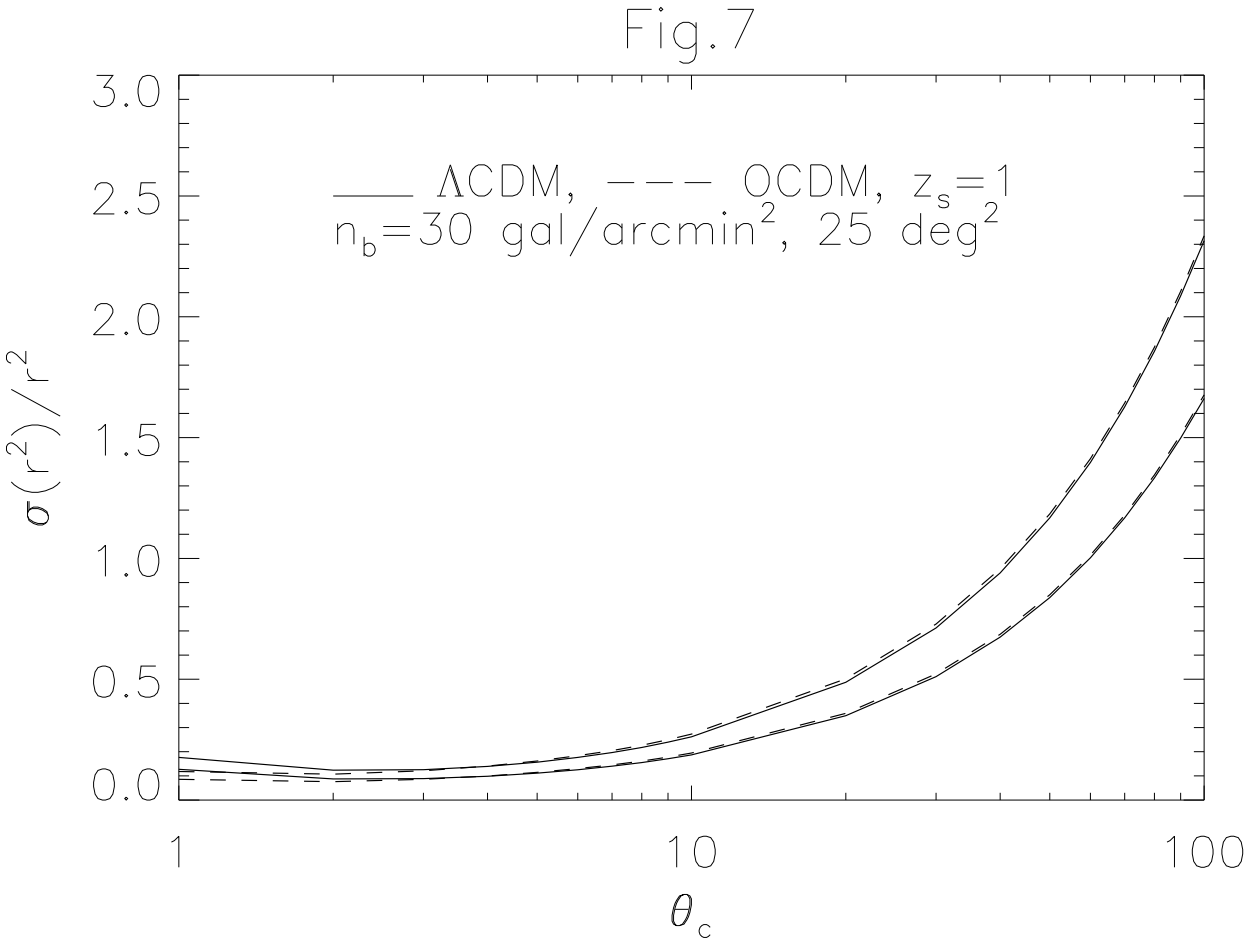

Fig. 7.— Plot of $\sigma(r^2)/r^2$ vs. θ_c (arcmin) with a survey area of 25 deg^2. All the other parameters are the same as in Fig.6.

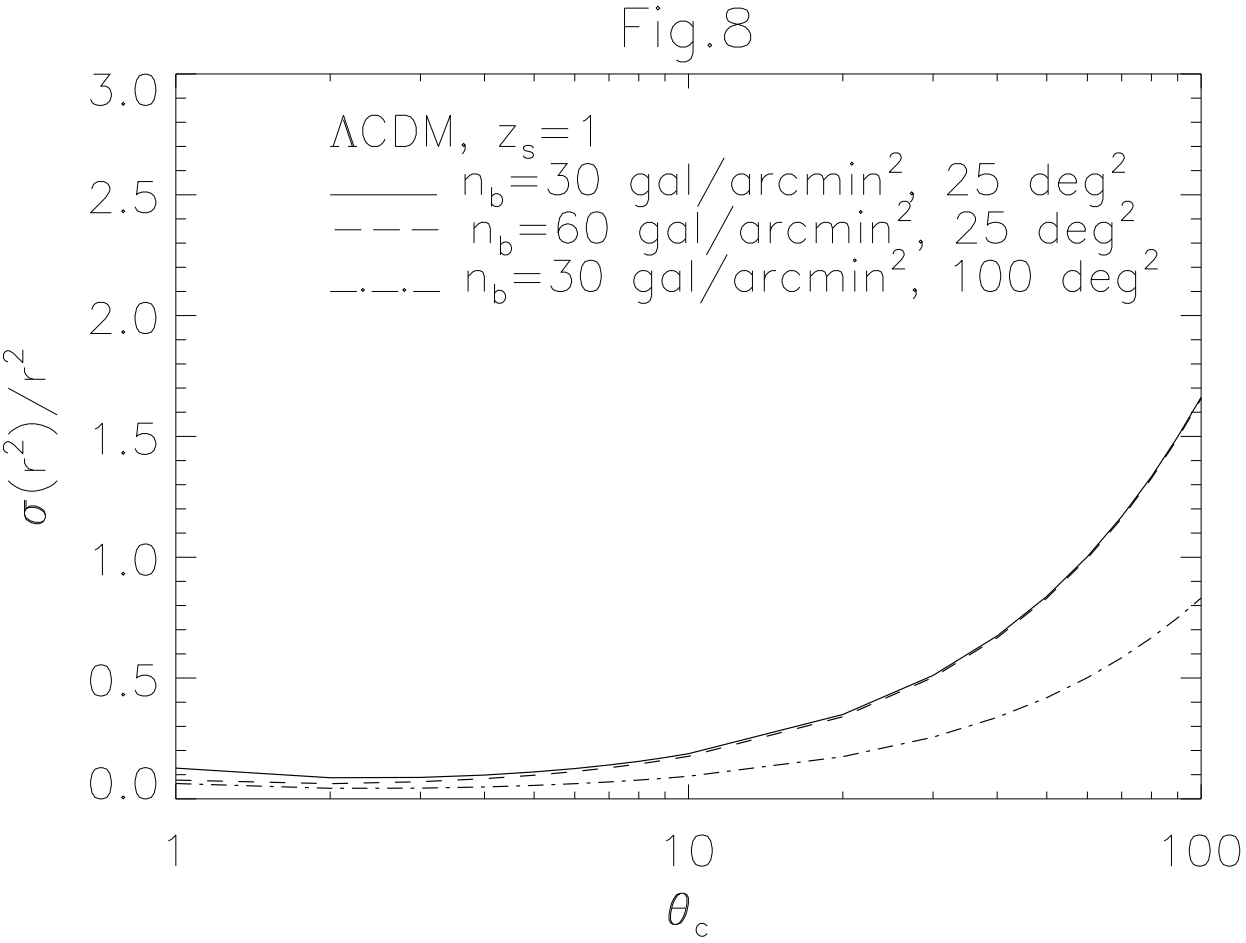

Fig. 8.— Plot of $\sigma(r^2)/r^2$ vs. θ_c (arcmin) for the ΛCDM model with $z_s = 1$ (eq.[22]). The solid line is for $n_b = 30$ gal/arcmin^2 and the survey area of 25 deg^2, the dashed line is for $n_b = 60$ gal/arcmin^2 and a survey area of 25 deg^2, and the dot-dashed line is for $n_b = 30$ gal/arcmin^2 and the survey area of 100 deg^2.

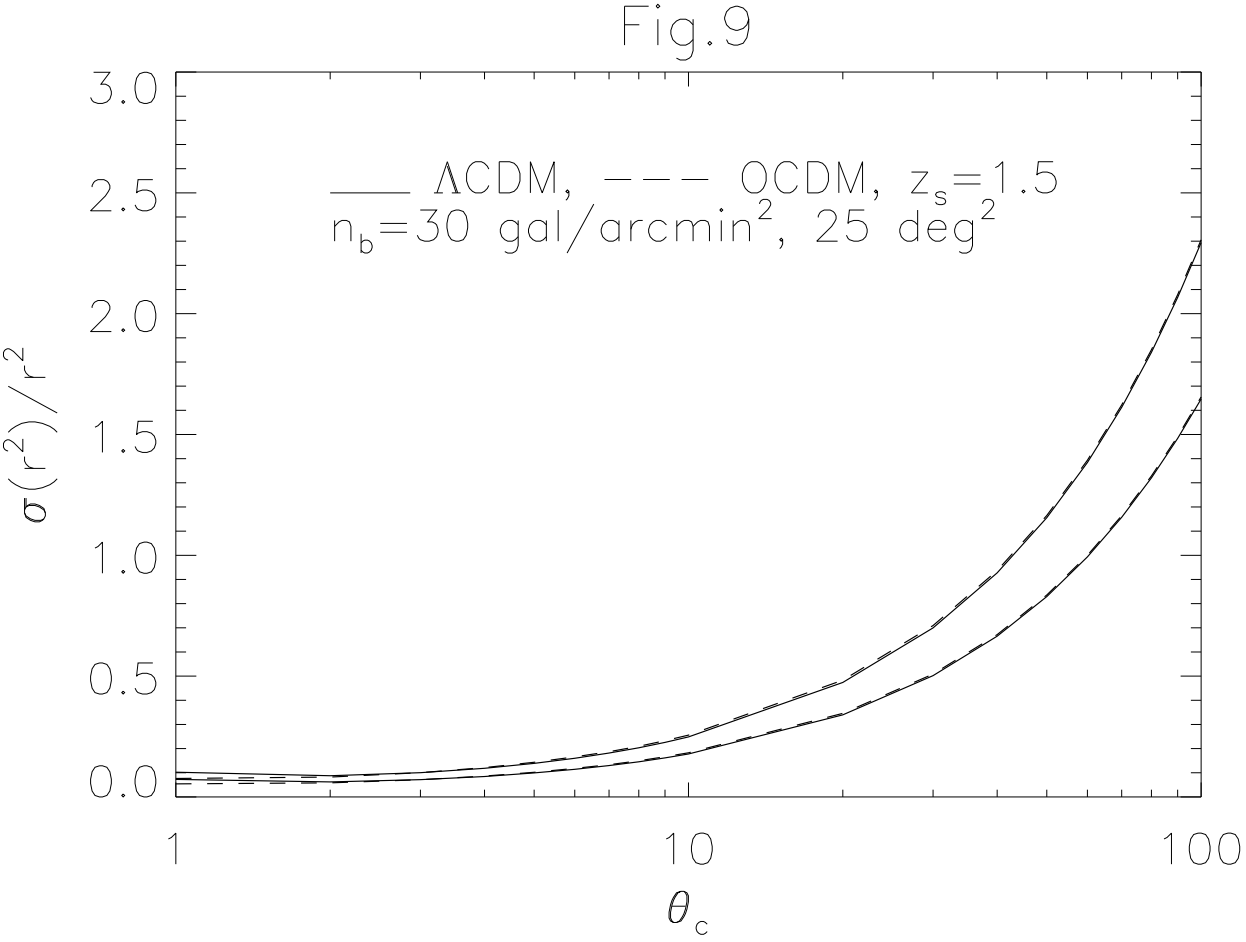

Fig. 9.— Plot of $\sigma(r^2)/r^2$ vs. θ_c (arcmin) with $z_s = 1.5$, $n_b = 30$ gal/arcmin^2, $n_f = 5$ gal/arcmin^2, and $\sigma_\epsilon = 0.2$. and a survey area of 25 deg^2. The meanings of the lines are the same as in Fig.6.

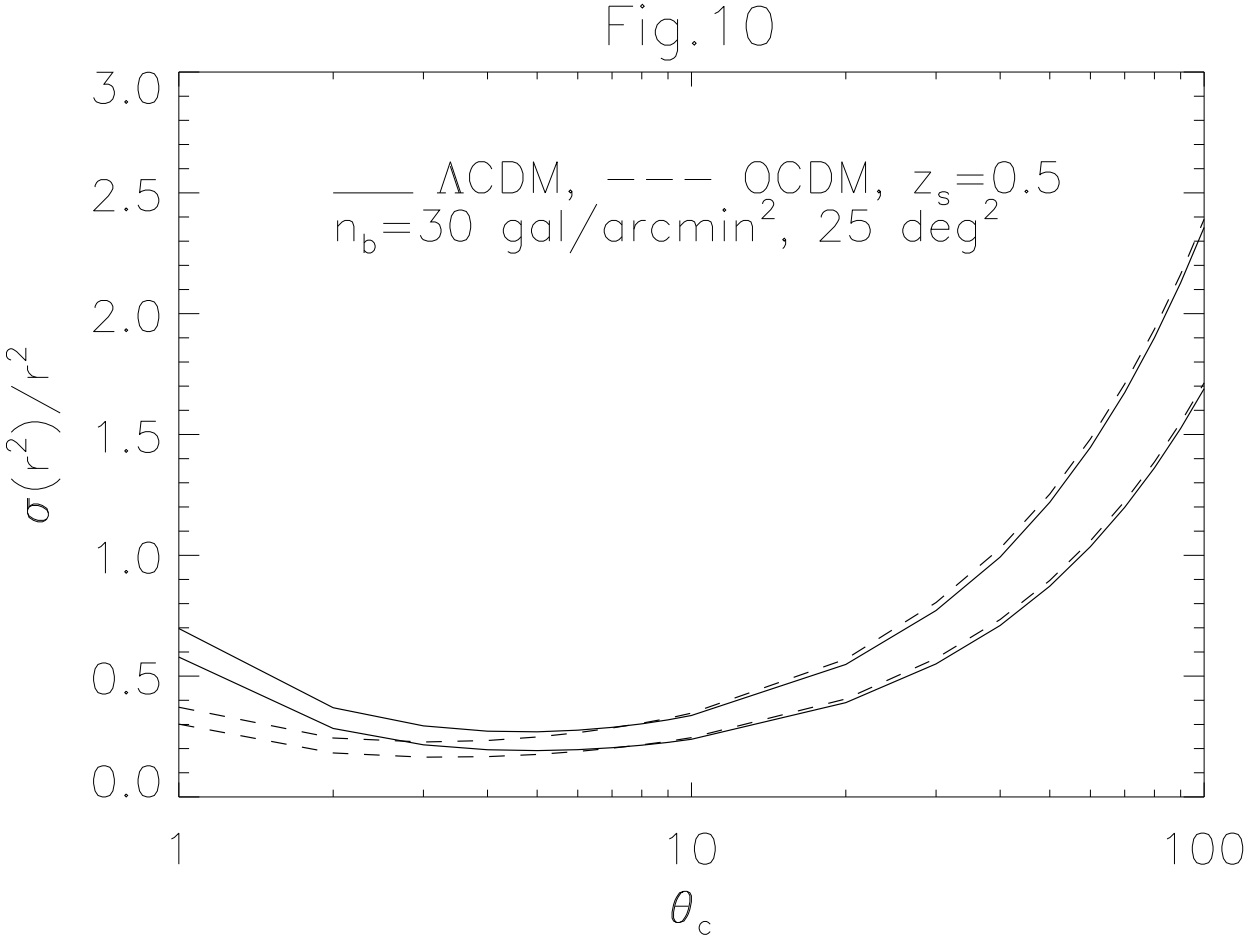

Fig. 10.— Plot of $\sigma(r^2)/r^2$ vs. θ_c (arcmin) with $z_s = 0.5$, $n_b = 30$ gal/arcmin^2, $n_f = 5$ gal/arcmin^2, $\sigma_\epsilon = 0.2$, and a survey area of 25 deg^2. The meanings of the lines are the same as in Fig.6.

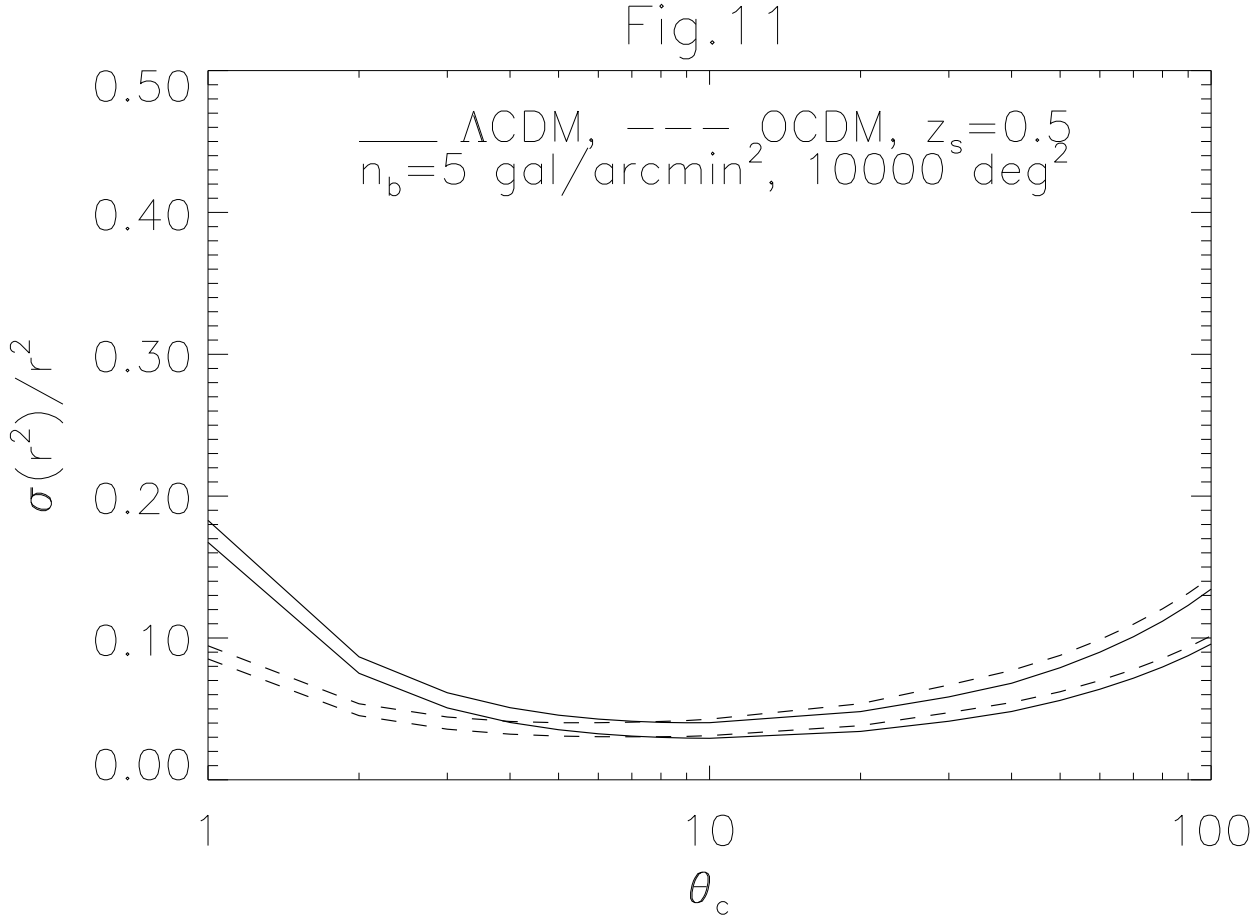

Fig. 11.— Plot of $\sigma(r^2)/r^2$ vs. θ_c (arcmin) with $z_s = 0.5$, $n_b = 5$ gal/arcmin^2, $n_f = 5$ gal/arcmin^2, $\sigma_\epsilon = 0.2$, and a survey area of 10^4 deg^2. The meanings of the lines are the same as in Fig.6.